Interaction between Surfaces with Attached Poly(ethylene oxide) Chains

Mikael Björling†

Physical Chemistry 1, Chemical Center, University of Lund, P.O. Box 124, S-221 00 Lund, Sweden

Received November 13, 1991; Revised Manuscript Received March 17, 1992

ABSTRACT: The paper presents a self-consistent mean-field lattice theory of the Scheutjens–Fleer type where segments may adapt to temperature and the local environment by changing their distribution among internal states. Some new features are introduced in the theoretical treatment of incompressible systems, and it is demonstrated how the chemical potential may be calculated without reference to a bulk system. The theory is applied to make a qualitative prediction for the interaction between surfaces with grafted poly(ethylene oxide), or PEO, chains. A simple two-state model for the PEO segments is used. The attractive force between the PEO-covered surfaces in water is predicted to be related to the temperature-dependent solubility of PEO in water. The contributions to the force are illustrated by simple examples. The attractive force does not change monotonically upon changing the graft density. At low coverages a strong bridging attraction is predicted if the surfaces are hydrophobic. As the surfaces become more polar, repulsion sets in at a larger separation and the overall attraction becomes less strong. A calculated, closed, solubility gap for a crude model of micelles of nonionic surfactants is presented.

1. Introduction

Controlling the stability of dispersions is very important in technological applications. It is the forces between the surfaces of the colloids that govern the stability, and polymers are increasingly used to modulate these forces.[1,2] A wealth of empirical observations of steric stabilization and destabilization by polymers is available.[2] Homopolymers generally destabilize dispersions thermodynamically but may slow down coagulation by increasing the viscosity. Physically attaching (grafting) polymers onto the surfaces yields thermodynamically stable dispersions in good solvent for the polymer segments, whereas flocculation is obtained in poor solvent. An analogous observation is made for diblock copolymers where one block strongly adsorbs to the surface. During recent decades a considerable number of theoretical investigations[3-65] and direct force measurements[66-82] have illuminated the situation, and a thorough understanding is emerging. This theoretical paper focuses on temperature-dependent forces between surfaces with grafted chains of poly(ethylene oxide) (PEO) in aqueous solution.

The surface force apparatus developed by Israelachvili[66] is a convenient method to measure forces under carefully controlled conditions and provides a testing ground for theories. A number of measurements have been performed on homopolymers in various solvents.[67-72] The behavior of diblock,[73-79] triblock,[80] and other[81,82] copolymers has been probed recently. Grafted polymers are less studied, but some of the diblock systems studied[73-76,78] can be regarded as such since one of the blocks adsorbs preferentially to the surface. While several of the researchers use polymers that contain EO groups, only a few use water as a solvent.[69,71,73,74,81,82] In some of these, the temperature dependence of the force has been studied.[73,74,81,82]

The theoretical treatments are based on scaling arguments and self-consistent-field (SCF) methods. The essential feature of a polymer is its connectivity. A simplified representation of an ideal polymer is therefore a path of a random walk. In the limit of a large number of steps (monomers) scaling predictions are obtained. On a more refined level of approximation, segments interact with (and/or exclude) each other and the polymer model becomes a path of a self-avoiding random walk performed in a potential field. If equilibrium properties are sought, it is reasonable to use a *mean* potential field produced by the ensemble average of the interactions with the rest of the system. This potential field is not known a priori, but one way to proceed is to build a theory where the distribution of segments (normally some average distributions) generates the mean field. The unknown potential can then be solved for by requiring self-consistence; i.e., the potential generated by the segment distribution must in its turn generate that same distribution. The solution is usually determined numerically because of the complex random walk in a field, but recently analytical results have become available.[28-37]

The self-consistent-field theories can be divided into two large groups: mean-field lattice models[38-52] or continuum space analogues.[3-37] The continuum theories are aimed toward treating very long chains and focus on the analogy between random walk and diffusion. In lattice treatments the random walk is constricted to a lattice and the explicit model on a segment level enables shorter chains to be modeled. In the limit of very long chains the two groups should be equivalent and differ mainly in the treatment of exchange repulsion, or excluded volume. Neglecting packing problems, it is approximated either by a constraint that requires that the local volume fractions sum to one[24,25,38-52] or by using the quadratic dependence on the local volume fraction for the excluded-volume interaction of pointlike segments due to Flory,[83] Edwards,[22] and de Gennes.[5] Since the latter implies infintely long polymers,[84] it is predominantly used in continuum models. An advantage of the latter approach was demonstrated recently when an analytical solution of the potential for long chains grafted to a surface could be obtained, thus avoiding the tedious search for self-consistence by numerical methods. Using an additional assumption of "strong stretching" suggested by Semenov[28] and Ohta[29] in the case of melts, Zhulina et al.[30-32] and Milner et al.[33-37] independently solved the problem which yields a parabolic potential. The agreement with numerical results is excellent in the case of long chains, but the neglect of loops becomes evident for shorter chains (around 200

† Present address: Physical Chemistry, Royal Institute of Technology, S-100 44 Stockholm, Sweden.

0024-9297/92/2225-3956$03.00/0

segments).[36] The volume fraction constraint is predominantly used in lattice models. It is a more straightforward method but necessarily demands a numerical solution. However, the lattice mean-field theories have the advantage that they are rather simple to adapt. The seminal papers of Scheutjens and Fleer[40,41] have subsequently been followed by a number of extensions and related theories.[42-65]

One such extension[48,52] includes internal degrees of freedom for the segments in order to use a model for PEO proposed by Karlström.[85] PEO and block copolymers containing PEO are widely used in industrial and pharmaceutical applications. The advantage of PEO lies not only in its relative hydrophilicity in spite of being uncharged but also in the fact that it shows a solubility gap in water as the temperature is increased. The temperature-dependent interaction provides an additional freedom of control that may be exploited. By allowing the segments of PEO to have internal degrees of conformational freedom, Karlström found a set of parameters[48,85] for a simple two-state model that gave a fair reproduction of the solubility gap. The internal state of PEO segments is represented by a balance between two conformational classes. One class is said to be predominantly polar and interacts well with water, while the other is nonpolar. In the model, the decreasing solubility in water (displayed by PEO) arises because the nonpolar class has more members than the polar class. As temperature increases, equipartition then gives the increasingly nonpolar character to the segments. Conformational changes with temperature are also corroborated by experiments (ref 86 and references therein) and encouraging results predicting adsorption of block copolymers.[52,87]

Since the notational complexity is not unduly increased by a general treatment, a different version of a previous extension[52] of the multicomponent formalism of Evers et al. (ESF)[49] is presented. A detailed knowledge of the theory is not necessary to understand the discussion in section 7. The theory relies by necessity on excessive notation (in spite of efforts to the contrary) but is a fairly standard procedure, and the main novelty is summarized here. All transformation of the parameters, previously introduced for numerical and notational reasons, is avoided to enhance interpretation. The numerical tricks are relegated to an appendix. As a consequence, it becomes clear how to calculate chemical potentials in incompressible systems *without reference to a bulk phase*. As stated, the aim of this paper is to investigate the temperature-dependent forces between surfaces with grafted PEO in water, but this is an additional twist. Previously a system could only be considered in equilibrium with homogeneous bulk, where expressions for the chemical potentials are readily available.[45,49-52,83] However, regarding a system as homogeneous in the traditional Flory sense[83] introduces serious errors for multicomponent systems, especially when components associate. The chemical potentials thus calculated may be completely unrelated to the real values they purport to reflect. Consider as an example diblock copolymers aggregating into micelles at very low concentrations. The chemical potential of the diblock copolymer (and the solvent) is obviously very different from that calculated for the corresponding homogeneous system. Even for a homopolymer in dilute solution, the chemical potential calculated in a mean field of spherical geometry is probably closer to reality than that calculated for the homogeneous system. In the lattice mean-field models (which are featured in this paper), heterogeneity is allowed in one dimension which is a less severe approximation.

The present paper is organized as follows: In sections 2 and 3 the general theory is presented. The segment interactions and the approximations involved are treated in section 4. The solution procedure is briefly described in section 5, where the practical details are found in the appendices: evaluation of segment and state distributions (B), numerical tricks (C) and analysis of conformations (D). The calculation of the free energy of interaction is dealt with in section 6. In section 7, the results and discussion start by considering the force between surfaces in simple systems and gradually extend to the complex system of grafted PEO chains. The paper finishes with some concluding remarks. The canonical chemical potential is introduced in section 3, its excess contributions are treated in section 4, and its calculation is described in section 6.

2. Partition Function

Consider a layered space of some specified geometry between two surfaces. The layers are numbered from i = 1 to M, with one surface at layer zero and the other at layer $M + 1$. The choice of geometry giving the lowest free energy requires either prior knowledge of the *real* system or physical intuition. Usually simple geometries like parallel plates, concentric spherical shells, etc., are tested. The types of components filling the system may range from simple solvent to heterogeneous chain molecules with internal degrees of freedom. The number of components of type x is denoted by n_x, and each component contains r_x connected segments. The segments may be of different types (species), labeled A, and each species may attain different states labeled B. (Some notational conventions are given in Appendix A.) The surfaces are treated as fixed distributions of surface species denoted 0 and $M + 1$.

Applying the Bragg–Williams approximation of random mixing within each layer reduces the scope of the problem to one dimension in the chosen geometry or, in other words, to finding *mean* number distributions of species and the *mean* fields generating them. In the lattice approximation all types of segments occupy sites of unit volume. Furthermore, the number distribution of segments is taken to be proportional to the volume fraction distribution. For consistency the layer spacing is then normally chosen to be on the order of a segment diameter, i.e., unity (mimicking close-packed layers). In what follows these approximations are implicit.

A matrix λ specifies the lattice topology, where λ_{ij} denotes the probability that a nearest neighbor to a site in layer i is in layer j. The neighbor relation described by the λ matrix is of course symmetric with respect to the number of nearest-neighbor pairs. Therefore, the elements of λ are subjected to a flux constraint that holds that the *total* number of nearest neighbors in layer j to sites in layer i, and vice versa, should be equal. Thus

$$L_i\lambda_{ij} = L_j\lambda_{ji} \tag{2.1}$$

where L_i is the number of sites in layer i. The flux constraint ensures that the λ matrix is physical in all geometries. The geometry itself is indeed parametrized by the set $\{L_i\}$ and the matrix λ. For completely flexible chains and in the lattice approximation, the λ matrix serves a dual purpose since it is also the matrix of normalized bond vector distributions. The bond length is on the order of the lattice spacing and consequently only the adjacent layers can be reached in one step. A rotationally symmetric bond distribution in planar geometry leads to $\lambda_{i,i} = 0.5$ and $\lambda_{i,\pm i} = \lambda_1 = 0.25$, the same as for a hexagonal lattice.

For curved surfaces such a simple analysis will yield a λ matrix which does not satisfy the flux constraint (eq 2.1). The effect of curvature must be simulated in an approximate manner. A reasonable assumption is that the number of bonds from layer i to $i+1$ is proportional to the area S_i separating them.[46,48] Using eq 2.1 and requiring the correct limit in the planar case, the most general solution is[48]

$$\lambda_{i,i+1} = \lambda_1 \frac{S_i}{L_i}, \quad \lambda_{i,i-1} = \lambda_1 \frac{S_{i-1}}{L_i}, \quad \lambda_{i,i} = 1 - \lambda_{i,i+1} - \lambda_{i,i-1} \tag{2.2}$$

where λ_1 is the bond distribution to the adjacent layer in the planar case.

Due to the random mixing approximation, segments can only be distinguished by the layer number of their occupancy. Conformations of chains can then only be distinguished as different *ordered* sequences of layer occupancy numbers. In the absence of segment–segment interactions (other than connectivity), both the components and the conformations are independent of each other. Let the statistical weight ω_{xc} of a conformation c of component x be the number of ways to place the first segment times the product of the bond vector probabilities of c

$$\omega_{xc} = L_{k(x,c,1)} \prod_{s=2}^{r_x} \lambda_{k(x,c,s-1),k(x,c,s)} \tag{2.3}$$

where $k(x,c,s)$ is the layer where segment s is located in conformation c. The statistical weight is then the number of ways to obtain the conformation c, divided by a constant factor that normalizes the bond vector distributions for component x. Choosing the product of all normalizing constants to be the reference, the ideal canonical partition function can be written as a sum over all specified sets of conformations $\{n_{xc}\}$

$$Q^{id} = \sum_{\{n_{xc}\}} \left\{ \prod_x \prod_c \frac{[\omega_{xc}]^{n_{xc}}}{n_{xc}!} \right\} \tag{2.4}$$

where n_{xc} is the number of component x in conformation c. The number of each component is kept constant, and the indistinguishability of chains in the same conformation has been taken into account. Each term in the ideal partition function is then proportional to the total number of distinguishable ways to realize the system in the absence of segment–segment interactions. Note that the selected reference here is different from Flory[83] and others.[49,52] Any choice of reference state is equivalent to dividing the ideal partition function by some constant. Flory[83] prefers a reference that corresponds to the product of the partition functions for the separated pure components. His choice is equivalent to scaling the number distributions to volume fraction distributions and removing a constant term (depending on the number of sites in the system) from the Helmholtz free energy. However, the choice is free as long as it is consistent. In this paper the number distribution becomes the central quantity and the implied lattice approximation is avoided. Other versions pick a reference which scales the number distributions to probabilities.[53-61]

Real systems are more complicated since segments may interact with each other and may have internal degrees of freedom adapting to the local environment. Furthermore, they can be subjected to constraints such as segment–segment excluded volume, impenetrable surfaces, and/or confined chain ends. The free energy contributions from these interactions (the excess free energy,[90] A^{ex}) are complex and must be approximated in the self-consistent-field treatment. These problems are deferred to section 4, and the canonical partition function is symbolically written as

$$Q = Q^{id}Q^{ex} = \sum_{\{n_{xc}\}} \left[\prod_x \prod_c \frac{\omega_{xc}^{n_{xc}}}{n_{xc}!} \right] e^{-\beta A^{ex}(\{n_{xc}\})} \tag{2.5}$$

where $\beta = [k_B T]^{-1}$, and each set is Boltzmann weighted by its excess free energy. Clearly, any set violating a constraint should be weighted by zero.

3. Equilibrium Distribution

At equilibrium, the most probable set of conformations ($\{n_{yd}\}$) which maximize Q will dominate. Introducing the *canonical* chemical potential (with pressure dependence removed; cf. section 6.2), which we denote η to distinguish it from Gibbs' chemical potential μ, the above condition can be rephrased so that the chemical potential η_y for any component y is equal for all conformations. The concept of chemical potential might seem artificial in an incompressible lattice system, but η plays the same role as μ and satisfies the Gibbs–Duhem type relation

$$A = \sum_y n_y \eta_y \tag{3.1}$$

where A is the Helmholtz free energy. Using the definition of (canonical) chemical potential[91] and the stated condition for equilibrium, the following relation must hold:

$$\beta\eta_y = \beta\eta_{yd} = \frac{\partial(-\ln Q)}{\partial n_{yd}} = \ln\left(\frac{n_{yd}}{\omega_{yd}}\right) + \beta\eta_{yd}^{ex} \tag{3.2}$$

with η_{yd}^{ex} defined by

$$\eta_{yd}^{ex} = \frac{\partial A^{ex}(\{n_{xc}\})}{\partial n_{yd}} \tag{3.3}$$

The excess chemical potential for a component (η_{yd}^{ex}) can be interpreted as the interaction free energy of a component y fixed in conformation d with a canonically averaged system. Using the probability of a conformation d of component y ($P_{yd} = n_{yd}/n_y$) and rearranging eq 3.2 yields a constitutive relation valid at equilibrium for all P_{yd}

$$P_{yd} = \frac{C_y}{n_y} \omega_{yd} \exp[-\beta\eta_{yd}^{ex}] \tag{3.4}$$

where the constant C_y is $\exp(\beta\eta_y)$. Since the probabilities should add up to unity, summing over all possible conformations d yields

$$\frac{C_y}{n_y} = [\sum_d \omega_{yd} \exp[-\beta\eta_{yd}^{ex}]]^{-1} \tag{3.5}$$

Thus, C_y/n_y is simply a constant of normalization. A self-consistent *equilibrium* probability distribution $\{P_{yd}\}$ can be found by requiring that eq 3.4 is satisfied for any component y and conformation d in the set. This procedure is described in section 5 and Appendix B.

4. Contributions to the Excess Chemical Potential

For components consisting of several segments, the excess chemical potential defined by eq 3.3 is conveniently approximated by the sum of the contributions from each of its segments

$$\eta_{yd}^{ex} = \sum_{s=1}^{r_y} \eta_{t(y,s),k(y,d,s)} = [\sum_{s=1}^{r_y} u_{t(y,s),k(y,d,s)}] + V_{yd}^{constraint} \tag{4.1}$$

where $t(y,s)$ is the species type of segment s in component

y and where we separate the external constraints from the interactions. External constraints are imposed by impenetrable surfaces or confined chain ends. For flexible, possibly end-confined, chains in a slit, the external constraint potential simply attaches an infinite cost to placing segments *inside* hard walls and/or to releasing confined segments; otherwise, it is zero. This approach is more general than the absorbing boundary conditions proposed by Silberberg[89] but has the same effect.

The term in the square brackets only depends on segment type and layer number. The segment potential u_{Ai} is the cost in excess free energy when a free monomer (segment) of type A is placed in layer i. Taking into account only the contributions from the nearest-neighbor interactions, the internal free energy, and the site–site excluded-volume constraint (U, A_{int}, and V_{hs}, respectively), the segment potential is obtained by the formal derivative

$$u_{Ai} = \frac{\partial[U + A_{int} + V_{hs}]}{\partial n_{Ai}} \tag{4.2}$$

where n_{Ai} is the number of segments of type A in layer i. Since random mixing of species within each layer is assumed, the above contributions are necessarily approximated by their mean-field counterparts.

A simple model for adaptation of species (segments) to the local environment is to allow for internal degrees of freedom. The adaptation is then described by changes in the distribution among internal states of a species. If states interact differently with the surroundings, the species may harmonize with it by changing state accordingly. Choosing one state as the reference (ensuring zero internal free energy for species lacking this degree of freedom), a relative internal free energy can be associated with each state. It is decomposed[48,52] into an energetic and an entropic term where the possible degeneracy of internal states is taken into account. The total internal free energy A_{int} is then expressed by

$$\beta A_{int} = \sum_i \sum_A n_{Ai} \sum_B P_{ABi} \left[\beta U_{AB} + \ln \frac{P_{ABi}}{g_{AB}} \right] \tag{4.3}$$

where P_{ABi} denotes the average probability that species A in layer i is in state B, U_{AB} is the relative internal energy for state B of species A, and g_{AB} is the relative degeneracy of state B of species A. The distributions of internal states are chosen such that the free energy is minimized for a given distribution of species (Appendix B). Evidently, allowing species to adapt always lowers the free energy relative to the case where segments cannot adapt.

In the lattice approximation the nearest-neighbor interaction energy (U) is a function of the average distributions of species and states. Choosing the reference energy to be that of the separated species, U can be reduced to an energy of mixing. This reference is more convenient than the energy reference previously chosen[49,52] with respect to separated heterogeneous components. Using the familiar Bragg–Williams χ parameters ($kT\chi_{CD} = w_{CD} - 0.5(w_{CC} + w_{DD})$, where w is a free energy of interaction but is treated as purely energetic in this paper) then yields

$$\beta U = \beta[U_{mix} + U_{surf}] = \frac{1}{2} \sum_i \sum_A \sum_B \sum_{A'} \sum_{B'} n_{Ai} P_{ABi} \chi_{BB'} \langle P_{A'B'i} \Phi_{A'i} \rangle + \sum_A \sum_B (\chi_{B0} \langle P_{AB0} n_{A0} \rangle + \chi_{B,M+1} \langle P_{AB,M+1} n_{A,M+1} \rangle) \tag{4.4}$$

where Φ_{Ai} is the volume fraction of A in layer i, and $\chi_{BB'}$ is the parameter of interaction between a species A in state B with a species A′ in state B′. The first term U_{mix} arises from interactions between the species and the second term U_{surf} from interaction with the surfaces. The surfaces are treated as step function distributions of "surface species", and $\chi_{B0}(\chi_{B,M+1})$ is the interaction parameter of species A in state B with the surface at layer 0 ($M + 1$). The bracketed $\langle P_{A'B'i} \Phi_{A'i} \rangle$ denotes the probability that a species A′ in state B′ is a nearest neighbor to a site in layer i. The probability of having type x as a nearest neighbor from layer i is $\langle x_i \rangle \equiv \sum_j \lambda_{ij} x_j$, where the sum is running over all possible connections from layers j to i. The angled brackets in the surface term denote the *number* of nearest neighbors of a certain type to a surface species.

Segment–segment excluded-volume (hard-sphere) interactions pose serious problems in the mean-field approximation since they are strictly local. However, it is convenient to approximate the condition of no overlap by a volume filling constraint for each layer on the equilibrium distribution of species:

$$\sum_A n_{Ai} L_i, \quad \forall i \tag{4.5}$$

Using the Lagrangian multipliers α_i, V_{hs} in eq 4.2 can then be cast in a mean-field form by

$$V_{hs} = \sum_i \alpha_i [L_i - \sum_A n_{Ai}] \tag{4.6}$$

where the undetermined multipliers α_i should be chosen to fulfill eq 4.5. The same approach has previously been used by several workers.[24,49–65] The contribution from V_{hs} to the excess free energy is zero when the constraints are satisfied as expected. Each α_i can be interpreted as a constraint pressure operating on each site (unit) volume to yield pressure–volume work. The Lagrange multipliers are in fact[58] similar to the lateral pressures introduced by Marčelja[53] and Gruen.[54] Using the pressure interpretation, one concludes that only the relative levels in the set $\{\alpha_i\}$ are important for the fulfillment of eq 4.5. In other words, only $M - 1$ α_i are independent. However, the absolute level for the *equilibrium* set $\{\alpha_i\}$ can be fixed by using the additional Gibbs–Duhem relation (eq 3.1). (See section 6.)

The derivative in eq 4.2 can now be evaluated. Using eqs 4.3, 4.4, and 4.6, the segment potential becomes

$$\beta u_{Ai} = -\alpha_i + \sum_B \sum_{A'} \sum_{B'} P_{ABi} \chi_{BB'} \langle P_{A'B'i} \Phi_{A'i} \rangle + \left\{ \sum_B P_{ABi} \left[\beta U_{AB} + \ln \frac{P_{ABi}}{g_{AB}} \right] + \lambda_{0i} \chi_{B0} P_{ABi} + \lambda_{M+1,i} \chi_{B,M+1} P_{ABi} \right\} \tag{4.7}$$

5. Self-Consistent-Field Solution

In order to calculate the species distributions for systems with heterogeneous polymers, the distributions of segments according to rank must be extracted from eq 3.4, i.e., the distributions of the first segment, the second segment, and so on. The self-consistent solution is obtained iteratively: For a given guess of the species' excess chemical potentials $\{\eta_{Ai}\}$, species' distributions $\{n_{Ai}\}$ are calculated using eq 3.4 (Appendix B). The approximations introduced in section 4 provide a link in the reverse direction from $\{n_{Ai}\}$ to $\{\eta_{Ai}\}$ through eqs 4.1 and 4.7, and a set $\{\alpha_{Ai}'\}$, required for eq 4.7 to hold, can be calculated. During the iteration, α_i' may vary between species, but in the final solution it must be the same for all species. (The prime reminds us that only the relative levels in $\{\alpha_i\}$ may be

determined by self-consistence.)

The self-consistent solution is reached if all the volume-filling constraints

$$L_i - \sum_A n_{Ai} = 0, \quad \forall i \tag{5.1}$$

are fulfilled *and* each α_i' is independent of species.

$$\alpha_{Ai}' - \alpha_i' = 0, \quad \forall A \tag{5.2}$$

During the iterations, $\{\alpha_i'\}$ is taken to be the species average of $\{\alpha_{Ai}'\}$. The variation of $\{\eta_{Ai}\}$, until eqs 5.1 and 5.2 are satisfied, is performed by a Newton–Raphson procedure.[92] The solution procedure involves using several numerical tricks, some of which are discussed in Appendix C.

6. Helmholtz Free Energy and Grand Potential

6.1. Fixed Number of Components. The Helmholtz free energy is

$$A = -k_B T \ln Q = U - TS + A_{int} \tag{6.1}$$

where the internal free energy (A_{int}) and the interaction energy (U) are given by eqs 4.3 and 4.4. It is obvious that the constraints should give no *direct* contribution to the free energy. The entropic part (TS) is obtained through Q^{id} in eq 2.4, evaluated with the equilibrium distribution as the only possible set. It is then given by

$$-\beta TS = \sum_y \sum_d n_{yd}\left[\ln\left(\frac{n_{yd}}{\omega_{yd}}\right) - 1\right] \tag{6.2}$$

The entropic contribution in eq 6.2 is difficult to evaluate since it entails summation over all possible conformations in the equilibrium set. A more tractable formulation can be obtained using the Gibbs–Duhem relation in eq 3.1 and the canonical chemical potential given by eqs 3.2, 4.1, and 4.7,

$$\beta\eta_y = \beta\eta_{yd} = \ln\left(\frac{n_{yd}}{\omega_{yd}}\right) + [\sum_{s=1}^{r_y} u_{t(y,s),k(y,d,s)}] \tag{6.3}$$

when all constraints are satisfied. Inserting eq 6.3 into eq 3.1 and simplifying using eqs 4.3, 4.4, and 6.2 gives as an intermediate step

$$\beta A = \sum_y n_y \beta\eta_y = -\beta TS + [\sum_y n_y] - [\sum_i L_i\alpha_i] + \beta[U + U_{mix}] + \beta A_{int} \tag{6.4}$$

Rearranging eq 6.4 and using $\beta\eta_y = \ln C_y$, the Helmholtz free energy can be written as

$$\beta A = \beta[U - TS + A_{int}] = \sum_y n_y\{\ln C_y - 1\} + [\sum_i L_i\alpha_i] - \beta U_{mix} \tag{6.5}$$

provided that a self-consistent solution has been reached. Equation 6.5 is independent of the absolute level in $\{\alpha_i\}$ since C is linked to α through eqs 3.5, 4.1, and 4.7. As a result we can in eq 6.5 directly use the raw, shifted quantities $\{C_y'\}$ and $\{\alpha_i'\}$ obtained from the solution procedure.

Comparison of eq 6.4 with eq 6.1 yields the identity

$$\sum_i L_i\alpha_i = \beta U_{mix} + \sum_y n_y \tag{6.6}$$

that establishes the absolute level of the constraint pressures as discussed above. The main advantage of this is that an unambiguous evaluation of the canonical chemical potentials becomes possible. Consider the case where the shift in the absolute level of α is P (the notation implies the equivalence between shift and pressure established in the next section). Denoting the shifted quantities by primes, the canonical chemical potential is given by

$$\eta_y = k_B T[\ln C_y] = k_B T[\ln C_y' + r_y P] \tag{6.7}$$

where P is obtained by insertion of $\alpha_i = \alpha_i' + P$ into eq 6.6

$$P = \frac{[\sum_y n_y] + \beta U_{mix} - [\sum_i L_i\alpha_i']}{\sum_i L_i} \tag{6.8}$$

Thus, both the free energy and the *canonical* chemical potential can be evaluated if the set $\{u_{Ai}\}$ is self-consistent.

6.2. Components in Equilibrium with Another System. The above treatment is valid for the canonical ensemble where the number of each component is fixed. It is simple to extend it to cases where one or more components in the system of interest (system one) are in equilibrium with a second system (system two). System two is assumed to be very much larger than system one so that it will remain virtually unchanged by the equilibrium. Consider a system where z components are in equilibrium. Changing from a canonical ensemble $Q(\{n_z\},V,T)$ to an ensemble $\Xi(\{n_y\},\{\mu_z\},V,T)$, the relevant free energy becomes the grand potential[91] Ω_G. It is given by a Legendre transformation to be

$$\Omega_G = A - \sum_z n_z\mu_z \tag{6.9}$$

where A is given by eq 6.5.

The fixed Gibbs chemical potentials μ_z are introduced into the theory by fixing C_z to $\exp(\beta\mu_z)$ (instead of $\exp(\beta\eta_z)$ as above) and adjusting n_z to satisfy eq 3.5. As evident from a Legendre transformation from Helmholtz to Gibbs free energy, μ_z will in general differ from η_{z1} by a pressure term

$$\mu_z = \eta_{z2} = \eta_{z1} + r_z P \tag{6.10}$$

where P is defined as a hypothetical pressure difference between the systems. (Note that r_z has units of volume.) By definition the pressure in system two is zero, so μ_z is equal to η_{z2}. The main advantage of eqs 6.7 and 6.8 is that we can consider direct equilibria with a canonically specified system two, instead of specifying the chemical potentials approximately via bulk approximations[45,52] (see Appendix E). Note that the *same* P is applied to all z components in equilibrium and that eq 6.10 is satisfied by changes in η_{z1} when several components are in equilibrium. In line with the discussion in section 6.1, it is clear that the pressure imposed by fixing one or more chemical potentials μ_z is equivalent to specifying the level of α. Since the self-consistent set $\{\eta_{Ai}\}$ in section 5 is independent of the level, the solution procedure described can still be used with the new choice of C_z. Furthermore, the resulting equilibrated system may be treated as a canonical ensemble to evaluate η_{z1} and P using eqs 6.7 and 6.8.

For the simple case when system two is a pure monomer solvent and $\beta\mu_z = -1$ (cf. Appendix E), subtraction of the chemical potential in eq 6.9 simply removes the dependence on the number of solvent molecules from Ω_G. Two coexisting phases have no pressure difference, so the *canonical* chemical potentials must be equal. The force between two surfaces at a separation D is related to the free energy of interaction, which is defined by the difference

in grand potential as two surfaces are brought from infinite separation to a separation of D layers

$$\Delta\Omega_G(D) = \Omega_G(D) - \Omega_G(\infty) \tag{6.11}$$

where "infinity" represents any separation where the surfaces do not interact.

For planar surfaces, the free energy of interaction is conveniently expressed per lattice site (W), which can be related to the normalized force (F/R) measured between the crossed cylinders of a surface force apparatus using the Derjaguin approximation[93]

$$\frac{\Delta\Omega_G}{La_s} = \frac{W}{a_s} = \frac{F}{2\pi R} \tag{6.12}$$

where the surface area is given by the number of sites in a layer (L) multiplied by the real cross-sectional area (a_s) of a lattice site and R is the radius of the crossed cylinders.

The free energy of interaction can also be calculated for nonplanar systems in the cell model approximation,[94] previously used predominantly for highly charged systems.[95-97] By symmetry, the outer boundary is treated as a reflecting surface since the number of components is the same in all cells. The reflecting boundary may be placed at the layer boundary or in the middle of a layer. In my calculations I have chosen only to place it at the layer boundary.

For aggregates in the cell model, an additional contribution to the grand potential due to mixing must be considered. Assuming that all other contributions are given by eq 6.9 and adding the ideal mixing entropy of the aggregates,[45] the total change in free energy for each cell of the system as the separation changes becomes

$$\Delta\Omega_G(D) = \Omega_G(D) - \Omega_G(\text{ref}) + kT \ln\left(\frac{\Phi_{agg}(D)}{\Phi_{agg}(\text{ref})}\right) \tag{6.13}$$

where Φ_{agg} is the volume fraction of the aggregate, i.e., the volume of the particle plus the volume of the attached chains divided by the total cell volume. In the cell model, a reference level must be chosen since at infinite aggregate separation the last term becomes infinite.

7. Results and Discussion

In what follows, the system is chosen to be planar with hard chains of length r grafted in equal numbers on both surfaces, i.e., with their first segment confined to the surface layer. The grafting density (σ) is the fraction of sites in a surface layer occupied by these first segments. In planar symmetry all layers have the same number of sites (L). The connection matrix (λ) is chosen to be equivalent to hexagonal symmetry for the nearest neighbors ($\lambda_{ii} = 0.5$ and $\lambda_{ii\pm1} = 0.25$ for all i and with all other entries equal to zero). As the surfaces approach each other, only solvent is extruded and thus the system may be treated as being in equilibrium with pure solvent. This simple choice avoids the problem of calculating the chemical potential for the chain–solvent system and gives the added advantage that the grand potential can easily be divided into energy and entropy contributions. Furthermore, the attractive van der Waals forces and the repulsive protrusion forces[98] are deemed small for the comparatively large surface separations considered.

Before focusing on the forces between PEO-covered surfaces, it is instructive to discuss simpler systems. Consider the case when the solvent and the surfaces are of the same nature as the segments, i.e., when the energy of interaction is zero (perfect solvent). As the surfaces near each other, grafted hard chains experience a loss of configuration space and the grand potential starts to increase when the segment distributions begin to overlap (Figure 1). For polymers the repulsion is sometimes divided into a conformational entropy and an "osmotic" contribution. For polymers, the former has been coined as an "elastic" contribution by de Gennes.[5] If the chains are forced to stay in the system by the action of a semipermeable membrane (instead of by grafting) and the system is sufficiently dilute to make the changes in the conformational entropy term negligible, the interpretation of the osmotic term agrees with the usual notion of osmotic pressure.

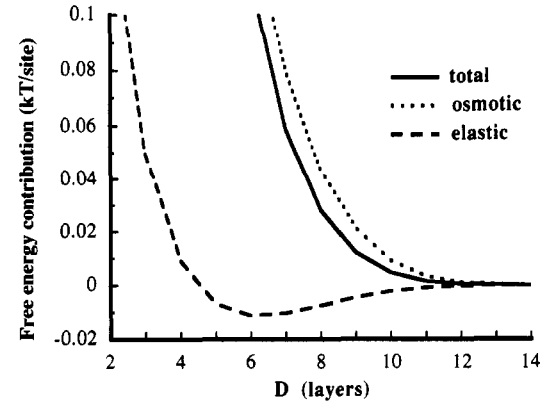

Figure 1. Grand potential (solid), with its elastic (dashed) and osmotic (dotted) contributions for grafted hard chains in perfect solvent. Chains are 10 segments long ($r = 10$) grafted on both planar surfaces with a grafting density $\sigma_s = \sigma_{s'} = 0.3$.

The osmotic contribution is purely repulsive and arises (in the mean-field theory) from the decrease in lateral entropy as the system becomes concentrated. An example of a system without an elastic contribution is constituted by grafted monomers, since they have no conformational entropy. Grafted monomers also illuminate one limitation imposed by the mean-field approximation. If the monomers were truly grafted to a point, no lateral movement would be permitted and the free energy of interaction would be zero or infinite upon overlap. An interpretation of a "grafted" chain is therefore that one end is confined to a surface layer and lateral motion is permitted.

The elastic contribution is due to accommodation of the conformational entropy of the grafted chains and is not monotonic (Figure 1). The repulsive contribution at short separations originates from the removal of possible conformations by the surfaces. It will only be important at low coverages when the surfaces can come close enough. The attractive contribution arises from the fact that the equilibrium set of chain conformations approaches that of an "ideal" polymer. Due to excluded volume and the inhomogeneous segment distributions, the grafted chains are strongly stretched. As the surfaces approach and the segment distributions overlap, the total distribution becomes more homogeneous and the conformations relax toward the "ideal" situation when the field has no direction. The phenomenon is identical to the "ideal" behavior of chains in a melt.[5,83]

It should be pointed out that the division of the free energy of interaction into osmotic and elastic contributions is somewhat arbitrary. Both are in fact two aspects of the same phenomenon: removal of configurational space. However, the division is commonly used in polymer theories. One important example is the Θ temperature for polymers in solution. At the Θ temperature the unfavorable osmotic contribution upon concentration of segments is canceled by favorable segment–segment interaction and the chains behave close to "ideally".

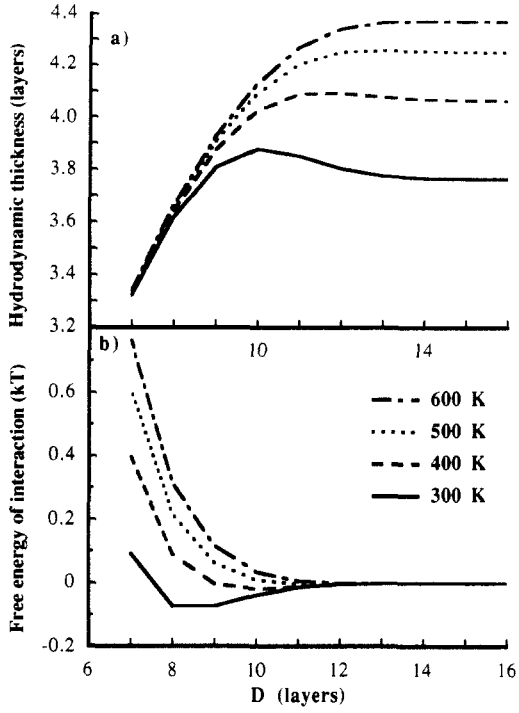

Figure 2. Hydrophobic chains on hydrophobic surfaces for different temperatures (r = 10, $\sigma_s = \sigma_{s'}$ = 0.3, $RT\chi_{WH}$ = 2.09, $RT\chi_{W0}$ = 10.0, and $RT\chi_{H0}$ = 4.44 kJ·mol^{-1}, where W denotes solvent, H chain species, and 0 either surface). (a) Hydrodynamic thickness δ_h for chains grafted on one surface. The increase in δ_h with increasing temperature due to stretching is consistent with decreasing hydrophobicity. Note the bridging at 300 K when the segment distributions on both surfaces start to overlap. (b) Free energy of interaction per site. The initial attractive force becomes repulsive as the solvent becomes better with increasing temperature.

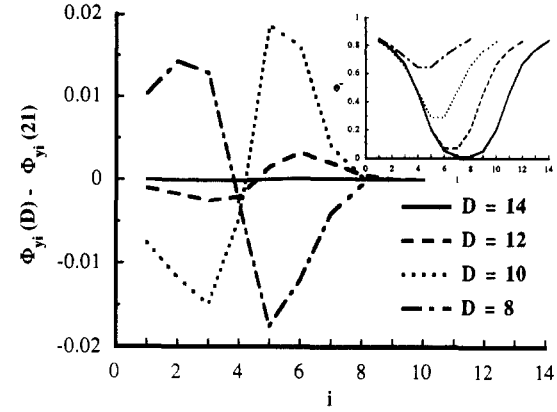

Figure 3. Change in the volume fraction distribution relative to the undisturbed distribution at D = 21 for chains on one surface at selected separations. The total volume fraction distribution is shown in the inset. Parameters are as in Figure 2, and T = 300 K.

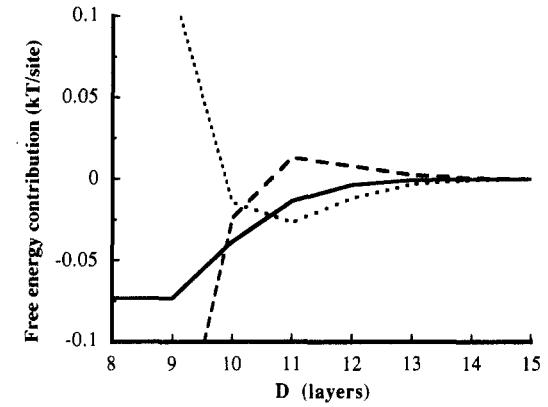

Figure 4. Free energy of interaction per site at 300 K from Figure 2b (solid), divided into its energy (dashed) and entropy (dotted) contributions. The initial "stretching" is entropically driven and gives a small attractive force. As the segment distributions continue to overlap the large attractive force is due to decreasing unfavorable segment–solvent contacts.

Next consider the case of hydrophobic chains grafted at high coverage on hydrophobic surfaces in an aqueous solvent (Figure 2a). Since the energy (eq 4.4) is given in kT units, raising the temperature is equivalent to decreasing the interaction parameters. Upon an increase of the temperature the initial attraction is transformed to repulsion as the system approaches the perfect solvent case. It was previously demonstrated by Van Lent et al.[47] that at high grafting densities attraction is obtained when the interaction parameter is greater than 0.5, i.e., approximately at the Θ temperature. This prediction is corroborated by force measurements.[67,70,77] As the surfaces approach each other the number of solvent–segment contacts are decreasing, and if these contacts are unfavorable, the gain in energy may dominate over the loss of entropy (cf. phase separation).

A convenient probe of the state of the grafted chains is the hydrodynamic thickness. The original theory[99] was developed for chains adsorbed on a *single* surface, and the hydrodynamic thickness δ_h is then a measure of the apparent layer thickness where solvent flow is obstructed. Since dangling tails affect the flow strongly, δ_h is dominated by extended tails. For grafted chains, δ_h is thus a measure of the level of "stretching" of the chains. The above concept of "hydrodynamic thickness" for chains on a single surface is convenient even when two surfaces are present. However, note that hydrodynamic thickness defined in this way does not correspond to a measurable quantity when the segment distributions overlap and only serves as a theoretical probe.

Since chains adsorbed only on *one* surface enter into the formula (Appendix D), bridging chains are excluded. When bridges form, they consequently contribute to a decrease of the hydrodynamic thickness. In Figure 2b, δ_h for chains grafted on *one* of the surfaces is calculated (Appendix D). In this case of high coverage, the number of chains bridging the two surfaces is negligible and δ_h reflects the true stretching. At 300 K, a subtle stretching of the chains occurs as the segment distributions begin to overlap, but at separations lower than nine layers the chains are compressed. The same fact is evident from Figure 3 where the changes in the volume fraction distributions at selected separations for chains on one surface, relative to the distribution at large separation, are displayed.

The inset in Figure 3 shows the total volume fraction distributions. Comparison shows that the segment distributions are relatively insensitive to the stress imposed by the approaching surfaces. The crucial test of theories for grafted polymers should therefore not be a correctly predicted volume fraction profile. A more sensitive test is the prediction of forces. Moreover, it is clear that the chains do "interdigitate" in contrast to the assumptions of Alexander[3,4] and de Gennes.[5-9]

By dividing the free energy of interaction into energy and entropy contributions (Figure 4), it becomes clear that the stretching gives rise to a weak entropy-favored attraction. Since the solvent dislikes both the chains and the surface, it tends to press the chains toward the surface. As the distributions start to overlap the chains can relieve the generated entropic stress, at an energetic cost, by stretching into the approaching segment distribution.

When the segment distributions start to overlap more, the main reason for the stronger attraction is the removal of unfavorable segment–solvent contacts. At short separations the entropy contribution dominates.

The stretching seen here is a weak cousin of the "bridging attraction" proposed by Scheutjens and Fleer[42] for homopolymers that adsorb strongly. It is slightly counterintuitive. The formation of bridges is entropically unfavorable in the ideal system, since *both* surfaces then remove configuration space. However, strong preferential adsorption of segments tips the balance. A clear-cut example with a strong bridging attraction is polyelectrolytes on oppositely charged surfaces.[100] At large surface separations, the chains are adsorbed onto the surfaces in flat configurations which is unfavorable in terms of the entropic contributions. As the surfaces come closer, the chains can alleviate this stress by binding to both surfaces, resulting in an attractive force between the surfaces. In this case, the stretching gives rise to an increase of physical bridges. A similar situation is demonstrated by triblock copolymers.[51,80] Triblock copolymers in a bad solvent for the end blocks can be regarded as chains with "sticky" ends in a simplified model. At large separations the chains are in a forced loop conformation, but as the configuration space increases when ends may bind on both surfaces at shorter separations attraction begins.

As mentioned in the Introduction, the Karlström model of PEO reproduces the solubility gap by allowing internal degrees of freedom. Specifically, segments are allowed to be in either of two states. One state is called polar (denoted P) and the other nonpolar (N) because of their differing interaction with the solvent (W). To drive the average state of the segments toward the nonpolar state with increasing temperature, the nonpolar state has a greater statistical degeneracy than the polar state. The parameters chosen gave a reasonable fit to the PEO–water concentration–temperature phase diagram. The interaction parameters were[48,85] $RT\chi_{WP} = 0.6508$, $RT\chi_{WN} = 5.568$, and $RT\chi_{PN} = 1.266$ kJ·mol^{-1}, with the internal free energy parameters $RTU_N = 5.086$ kJ·mol^{-1} and $g_N = 8$. The surfaces are chosen to be hydrophobic, and the interaction parameters are chosen to reflect this (see Figure 5). In order to compare the calculated properties with experimental results, the layer spacing must be estimated. Assuming the EO volume to be approximately 64 Å^3, the segments could be considered as cubes with a side length of 4 Å. The layer spacing is therefore close to 4 Å and the cross-sectional area is nearly 16 Å^2. Consequently, a free energy of interaction of 1 kT per surface site at 300 K corresponds to a normalized force (F/R) of 0.16 N/m (cf. eq 6.12).

For PEO chains grafted on hydrophobic surfaces, the free energy of interaction is related to the solubility gap in the PEO–water phase diagram (see Figure 5). The minimum in the free energy of interaction initially deepens with increasing temperature but then becomes more shallow at very high temperatures. At 400 K the segments are so hydrophobic that the grafted layer contracts as seen from the hydrodynamic thickness at large separations. The contraction is corroborated by experimental observations.[74] At higher temperatures, the unfavorable segment–solvent interactions become less important and the chains tend to approach ideal hard chains as in Figure 2.

As a comparison, a chain without internal degrees of freedom can be considered as being in an average state, where its interaction parameters then become average parameters. In fact, the parameters for the hydrophobic chains in Figure 2 were chosen as the average state that

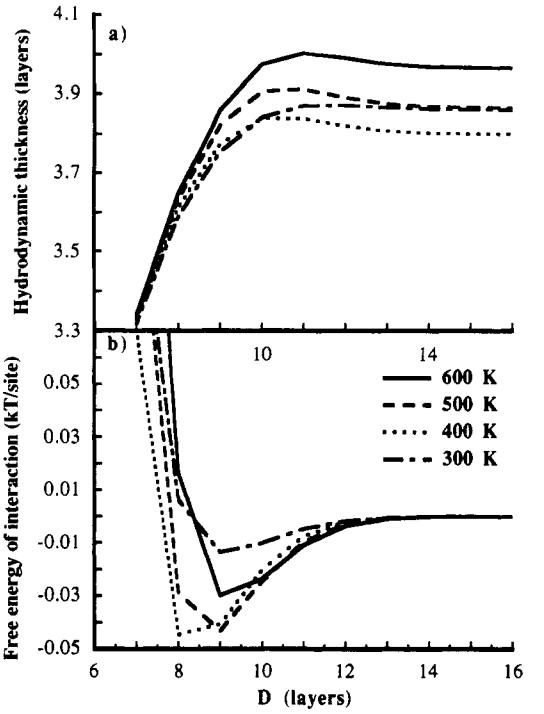

Figure 5. PEO chains on hydrophobic surfaces for different temperatures ($r = 10$, $\sigma_s = \sigma_{s'} = 0.3$, PEO interaction parameters (see text), $RT\chi_{W0} = 10.0$, $RT\chi_{P0} = 6.7$, and $RT\chi_{N0} = 3.5$ kJ·mol^{-1}, where W denotes solvent, P the polar state, N the nonpolar state, and 0 either surface). (a) Hydrodynamic thickness δ_h for PEO chains grafted on one surface. Note that the grafted layers are more compact at 400 K. (b) Free energy of interaction per site. With increasing temperature the interaction initially becomes more attractive, and then less so (cf. the solubility gap). The minimum is shifted to a smaller separation at 400 K.

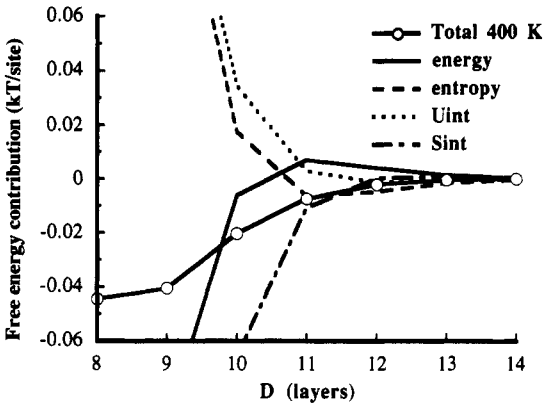

Figure 6. Free energy of interaction per site (solid, open circles) for PEO chains at 400 K as in Figure 5a. Its contributions can be divided into entropy (dashed), energy (solid), internal energy (dotted), and internal entropy (dash-dotted).

gave the best fit to the *segment distribution* of PEO chains at 300 K.[48] The free energy of interaction yields a much deeper minimum in Figure 2 for two reasons: first, the PEO segments can adapt at each separation and thus this lowers the free energy; second, the average state that gave the best fit for the segment distribution is more hydrophobic than the average PEO segment at 300 K.

Division of the free energy of interaction per site into contributions from entropy, energy, internal energy, and internal entropy at 400 K is shown in Figure 6. The same trends as in Figure 4 are seen, but here some of the unfavorable energetic interaction between water and PEO at large separations has been transferred to unfavorable internal entropy of the segments. As the two grafted layers start to overlap and the PEO–water contact is reduced, the internal strain due to adaptation is diminished, leading

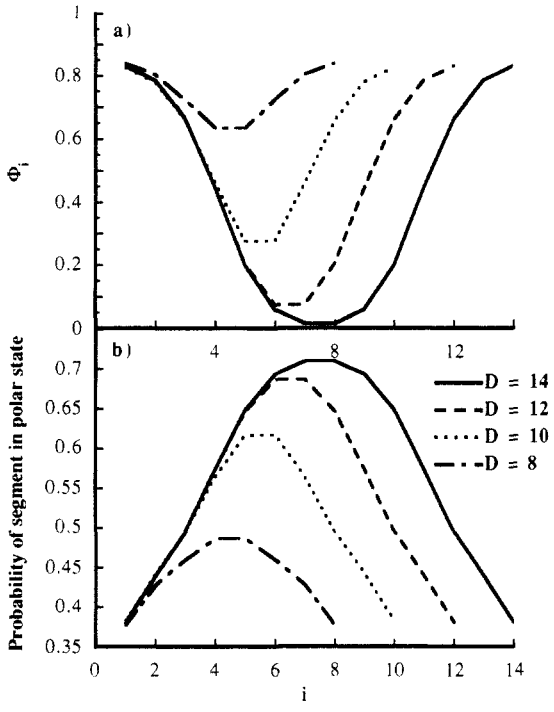

Figure 7. (a) Volume fraction profile and (b) internal state profile for PEO at 400 K for selected separations. Parameters are as in Figure 5.

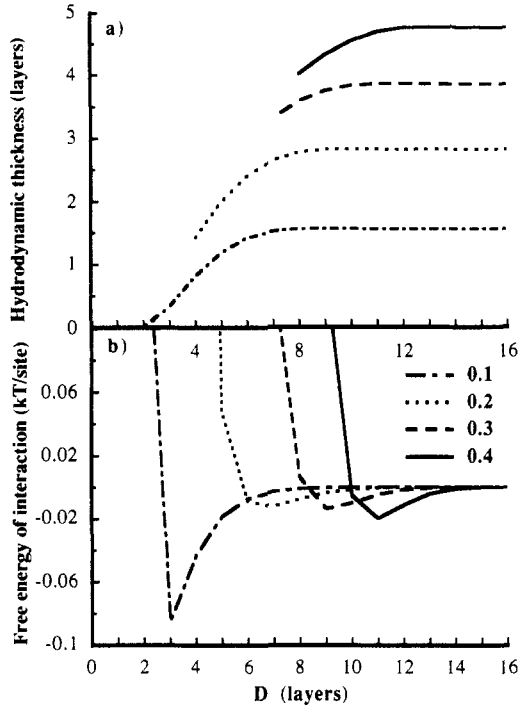

Figure 8. PEO chains on hydrophobic surfaces at selected coverages ($\sigma_s = \sigma_{s'} = 0.1$–$0.4$, other parameters are as in Figure 5). (a) Hydrodynamic thickness for PEO chains on one surface. (b) Free energy of interaction per site.

to a net negative (attractive) internal contribution to the free energy of interaction. Thus, in Figure 6 it is evident that the PEO segments adapt their conformational state to interact more favorably with the environment at the expense of internal entropy. This behavior is vaguely reminiscent of "hydrophobic" interaction and "water structure",[101] where unfavorable interaction with water is also alleviated at the expense of the orientation of the water molecules. It turns out that the internal free energy contribution is attractive, whereas the sum of the energy and entropy contributions is repulsive. Thus the main contribution to the attraction comes from the decreasing internal entropy contributions. Internal degrees of freedom essentially give the monomers the possibility of adapting to the local environment. That the state is a function of the local composition is clearly shown in Figure 7 at selected separations.

The influence of the surface coverage of grafted PEO chains on hydrophobic surfaces at 300 K is shown in Figure 8. The hydrodynamic thickness for low coverage $\sigma = 0.1$ (or 0.2) falls below 1.0 (2.0), indicating bridge formation. Analysis shows that this is indeed the case. For high coverages, a negligible number of bridges are formed. At the lowest graft density (0.1), the free energy of interaction is much stronger. It can be understood in terms of bridging attraction discussed above. At this low coverage the chains must be in rather flat configurations in order to expel as much of the water as possible from the hydrophobic surface. The adaptability of the PEO segments plays a role since it seems to allow for a greater density of segments in the layer close to the surface (the same trend is not shown for chains with the parameters from Figure 2).

The dependence on the character of the surface for low coverage (0.1) at 300 K is shown in Figure 9. At high coverages the surfaces behave predominantly as PEO itself, and the nature of the surfaces gives a negligible modulation. In order to minimize the number of parameters used, the surface species are chosen to be either hydrophobic, or a segment in nonpolar or polar state, or water (see above). The water dislikes the hydrophobic and nonpolar surfaces

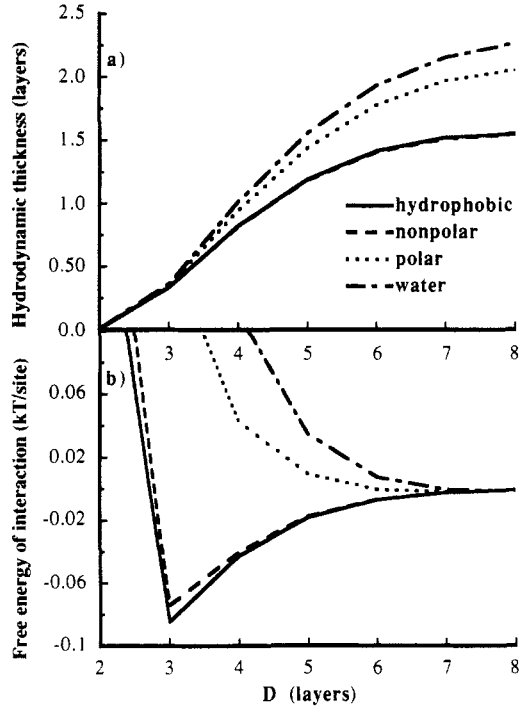

Figure 9. PEO on different types of surfaces at low coverage ($r = 10$, $\sigma_s = \sigma_{s'} = 0.1$). χ parameters in units of kJ·mol^{-1} for different surface species are as follows. Hydrophobic: $RT\chi_{W0} = 10.0$, $RT\chi_{P0} = 6.7$, and $RT\chi_{N0} = 3.5$. Nonpolar: $RT\chi_{W0} = 5.568$, $RT\chi_{P0} = 1.266$, and $RT\chi_{N0} = 0.0$. Polar: $RT\chi_{W0} = 0.6508$, $RT\chi_{P0} = 0.0$, and $RT\chi_{N0} = 1.266$. Water: $RT\chi_{W0} = 0.0$, $RT\chi_{P0} = 0.6508$, and $RT\chi_{N0} = 3.5$. Otherwise PEO parameters (see text). (a) Hydrodynamic thickness for PEO chains on one surface. (b) Free energy of interaction per site.

and forces the chains onto the surfaces, leading to a bridging attraction. For the polar and water surfaces, the attraction is very much smaller. The repulsion also starts earlier, as a consequence of the more stretched chains.

The direct force measurement performed by Claesson et al.[73] with the nonionic surfactant $C_{12}E_5$ (a dodecane

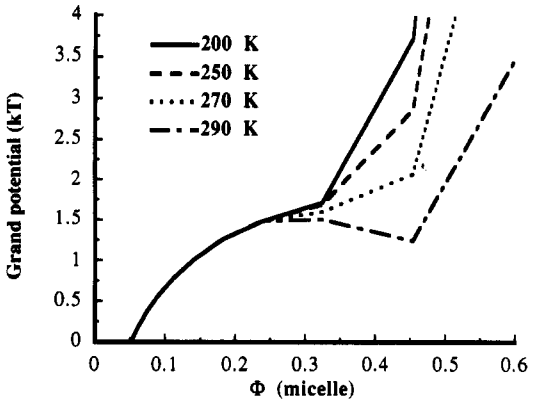

Figure 10. Grand potential near the lower consolute point for the $C_{12}E_{12}$ micelle model.

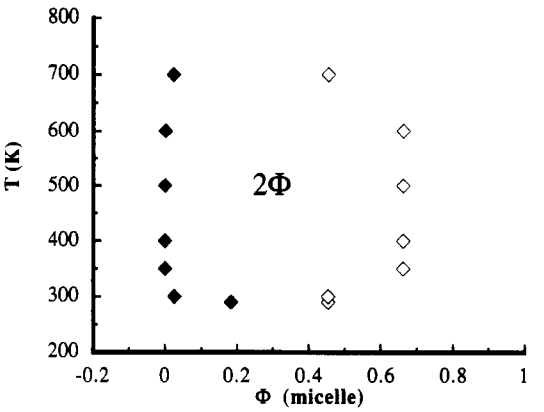

Figure 11. Calculated phase diagram for $C_{12}E_{12}$ micelles displaying the solubility gap in aqueous solution.

with five ethylene oxide segments) adsorbed on a hydrophobic surface prepared by the Langmuir–Blodgett technique is the closest system for comparison of the calculated free energy of interaction per site. The simple model adopted assumes that the hydrocarbon tail is embedded in a solid surface and that the EO tail can be regarded as grafted. Assuming a graft density comparable to a bilayer of $C_{12}E_6$[102] (with a calculated headgroup area of 47 Å^2, $\sigma = 0.34$), the onset of the measured repulsion was not consistent with simple volume-filling constraints. The coverage is probably lower if it is assumed that the surfactant remains on the "solid" surface. The calculated attractive force is about 10–20 times larger than the measured force. Furthermore, while trends in the temperature dependence of the calculated force are correct, the drastic changes in the measured force cannot be reproduced. The reasons for these discrepancies are many. First, the lattice approximation itself is rather crude for a chain as short as five segments. Furthermore, backfolding of chains is allowed in the model and consequently the repulsive contribution is underestimated. Second, in addition to being more complex than the simplified model, the experimental system contains salt due to incomplete neutralization of the surfaces after hydrophobization. This leads to double-layer repulsion and perturbations due to interaction of the salt with the surfactant and the solvent. The latter could also be a reason for the large changes in the measured force with temperature. Malmsten et al.[82] have less salt in their system, but on the other hand their polymer is heterogeneously ethoxylated.

Last, the concentration–temperature phase diagram of the nonionic surfactant $C_{12}E_{12}$ is considered. The micelle is viewed as a hydrophobic hard core with grafted ethylene oxide segments, and spherical symmetry is used. The crude model neglects the possible growth of micelles with increasing temperature,[104] but for $C_{12}E_{12}$ growth is probably negligible. Taking the radius of the core to be approximately that of a stretched C_{12} chain, 17.6 Å, and thus the number of grafted chains (aggregation number) to be 65, the phase diagram can be calculated by noting the concentrations of possible coexisting phases at different temperatures. Figure 10 shows such calculations for the lower phase boundary, where the separation D between aggregates has been transformed into the equivalent volume fraction of micelles. At 290 K the free energy of interaction performs a van der Waals loop and two phases at different concentrations coexist, i.e., the composition at the minimum and at the corresponding value of free energy of interaction. The system phase separates into a concentrated micellar solution in equilibrium with almost pure water. Combining the result of several calculations leads to the phase diagram displayed in Figure 11. While the qualitative behavior is correct, the quantitative agreement with experiment is less so. The experimental cloud point[103] is about 371 K. Furthermore, the calculated two-phase region is far too large. Most of the problem can be explained by the difficulty in probing the free energy of interaction at small separations because of the discrete layers implicit in the lattice model. The consequence is that neither the depth of the minimum nor the concentration where it is found is well determined. For longer chains these problems will be less severe.

8. Concluding Remarks

Some of the approximations introduced in the paper to simplify calculations can be remedied, at a cost. The complete flexibility of chains was introduced to enable a matrix method to be used. If bond angles are constrained and/or if each chain must be strictly self-avoiding, these problems can be treated by introducing a memory in the generation of chain conformations.[46,53–61,65] Due to the computational effort involved, these methods are restricted to short chains. An alternate interpretation of a "segment" in a completely flexible chain is as a Kuhn "blob".[5,23] The lattice spacing is then on the order of a Kuhn length, and the volume excluded by a site can be set to a number less than 1 since the blob is compressible. However, there is a limit for the useful refinements of the model on the molecular level (short of a full-scale simulation), since the random-mixing approximation introduces errors. Consequently, the simple lattice model is still useful for qualitative predictions since most of the important physics is intact.

The theoretical treatment presented here adds a number of new features to the extension of ESF[49] reported in a previous work.[52] The self-consistent solution using Lagrange multipliers, or constraint pressures, mixes important parameters in the system. The introduction of "canonical chemical potential" proves to be a convenient concept for the demixing, since a Gibbs–Duhem relation gives a natural constraint on the Lagrange multipliers. A simple expression for the free energy can be obtained (not new), and, more importantly, chemical potentials in incompressible systems can be calculated without reference to a bulk system. Furthermore, the formalism is such that it is simple to extend it to a nonlattice self-consistent-field theory for hard-sphere chains.[88]

The theory has been applied to surfaces with grafted polymers, and forces between such surfaces have been investigated. The model is found to be an excellent tool for promoting an understanding of the mechanisms involved. The poly(ethylene oxide) model (allowing internal degrees of freedom) gives reasonable qualitative

predictions in spite of its simplicity. Although it involves five parameters, some of them can be estimated by quantum mechanical calculations[85] and their functional relationship is fixed by the mechanistic interpretation of the model.

Acknowledgment. I thank Per Linse, Håkan Wennerström, Svante Nilsson, Jan Scheutjens, Olle Söderman, and Ulf Olsson for generous help. The National Swedish Board for Technical Development (STU) and Kungliga Fysiografiska Sällskapet i Lund are gratefully acknowledged for financial support.

Appendix A. Notation

Indices

A, A′	species (type of segment)
B, B′	type of state
c, d	conformation
i, j	layer number
H	hydrophobic segment
$k(x,s,c)$	layer where the segment of rank s of component x in conformation c is located
N	PEO segment in the nonpolar state
P	PEO segment in the polar state
s	segment rank
$t(x,s)$	species type of the segment of rank s belonging to component x
x, y	component
W	water or solvent
z	component in equilibrium
1, 2	systems in equilibrium with each other
0, $M+1$	denote surface layers and surface species

Variables

A	Helmholtz free energy, eq 6.1
A^{ex}	excess free energy of interaction, eq 2.5
A_{int}	total internal free energy, eq 4.3
C_y	$\exp(\beta\eta_y)$ or $\exp(\beta\mu_y)$, eq 3.4 or section 6
D	separation between surfaces or aggregates
G_{Ai}	species weighing factor, $\exp(-\beta\eta_{Ai})$, eq B.1
$\mathbf{G}^A$	diagonal matrix containing G_{Ai}
g_{AB}	degeneration of state B of species A
L_i	number of sites in layer i
n_x	number of component x
n_{Ai}	number of segments of type A in layer i, eq B.10
n_{xsi}	number of sites in layer i occupied by segments of rank s belonging to component x, eq B.8
P_{ABi}	fraction of species A in layer i which are in state B, eq B.13 and B.14
P_{xc}	probability of conformation c for component x, eq 3.4 or B.3
$\mathbf{g}(x,s)$	unnormalized number distribution of segments of rank s belonging to component x, eq B.6
Q	canonical partition function
Q^{ex}	interaction part of the canonical partition function, eq 2.5
Q^{id}	canonical partition function for a noninteracting system, eq 2.4
r_x	number of segments in component x
r_{xA}	number of segments of type A in component x, eq E.1
$\mathbf{s}$	column vector with unit elements
S	entropy, eq 6.2
U	total interaction energy, eq 4.4
U_{mix}	energy due to segment–segment interactions, eq 4.4
U_{surf}	energy due to segment–surface interactions, eq 4.4
U_{AB}	internal energy of state B of species A
u_{Ai}	segment potential for species of type A in layer i, eq 4.7
V_{hs}	excluded volume constraint, eq 4.6
$V_{yd}^{constraint}$	external potential acting on conformation d of component y
W	interaction free energy per surface site, eq 6.12
$\mathbf{W}^A$	transition matrix, eq B.4
α_i	Lagrangian multiplier related to volume constraints, eq 4.6
β	$[kT]^{-1}$ over Boltzmann's constant times absolute temperature
γ_{Ai}	Lagrangian multiplier related to the internal states, eq B.12
δ_h	hydrodynamic layer thickness
Δ_i	column vector with components δ_{ij} for all j
$\Delta\Omega_G$	free energy of interaction, eq 6.11
η_{Ai}	excess chemical potential of species A in layer i, eq 4.1
η_{xc}^{ex}	excess chemical potential for component x in conformation c, eq 3.2
η_x	canonical chemical potential for component x, eq 3.2
λ_{ij}	fraction of connections from layer i to layer j, eq 2.2
λ	connection matrix containing λ_{ij}
μ_x	grand canonical chemical potential of component x, eq 6.10
σ	grafting density
ϕ_{Ai}	fraction of sites in layer i occupied by segments of type A
ϕ_{yi}	fraction of sites in layer i occupied by segments belonging to component y
ϕ_{agg}	volume fraction of the micellar aggregate
$\chi_{BB'}$	Flory–Huggins interaction parameter between species A in state B and species A′ in state B′, eq 4.4
ω_{xc}	combinatorial factor related to the degeneracy of component x in conformation c neglecting self-exclusion, eq 2.3
Ω_G	grand potential, eq 6.9

Appendix B. Evaluating Equilibrium Distributions

B.1. Segment Distribution. The theory given is an extension of a previously presented method[48] to inhomogeneous polymers. Introducing the weight factors G_{Ai} defined as

$$G_{Ai} \equiv \exp[-\beta\eta_{Ai}] \tag{B.1}$$

eq 3.4 may be written as

$$P_{yd} = \frac{C_y}{n_y}\omega_{yd}\prod_{s=1}^{r_y} G_{t(y,s),k(y,d,s)} \tag{B.2}$$

where $t(y,s)$ denotes the species of segment s in component y. Decomposing ω_{yd} according to eq 2.3 yields

$$P_{yd} = \frac{C_y}{n_y}[L_{k(y,d,1)}G_{t(y,1),k(y,d,1)}] \times [\prod_{s=1}^{r_y} G_{t(y,s),k(y,d,s)}\lambda_{k(y,d,s-1),k(y,d,s)}] \tag{B.3}$$

which can be interpreted as a Markov process. Antici-

pating the matrix calculations to come, let the transition matrix be

$$(\mathbf{W}^{A})_{ij} \equiv G_{Ai}\lambda_{ji}, \quad \mathbf{W}^{A} \equiv \mathbf{G}^{A}(\lambda)^{T} \tag{B.4}$$

where $\mathbf{G}^{A}$ is a diagonal matrix with $(\mathbf{G}^{A})_{ii} \equiv G_{Ai}$ and $(\lambda)_{ij} \equiv \lambda_{ij}$. (Note that the superscript is a species label.) Identifying the second square bracket in eq B.3 with $(\mathbf{W}^{t(y,d)})_{k(y,d,s),k(y,d,s-1)}$ and the first square bracket with the entry $k(y,d,1)$ of an unnormalized distribution of the first segment $\mathbf{g}(y,1)$, eq B.3 may be expressed as a matrix multiplication in component form

$$P_{yd} = \frac{C_y}{n_y}[\prod_{s=2}^{r_y}(\mathbf{W}^{t(y,d)})_{k(y,d,s),k(y,d,s-1)}](\mathbf{g}(y,1))_{k(y,d,1)} \tag{B.5}$$

As a first step toward the reduction of eq B.5 to segment distributions, define the vector $\mathbf{g}(y,s)$ by

$$\mathbf{g}(y,s) = [\prod_{s'=2}^{s}\mathbf{W}^{t(y,s')}]\cdot\mathbf{g}(y,1) \tag{B.6}$$

where the order of the matrix multiplication denoted by the product is $\mathbf{W}^{t(y,s)}x\mathbf{W}^{t(y,s-1)}x...x\mathbf{W}^{t(y,3)}x\mathbf{W}^{t(y,2)}$. Each $\mathbf{g}(y,s)$ is related to the distribution of the segments of rank s but is not normalized. Note that the $\mathbf{g}(y,r_y)$ is the unnormalized probability distribution of the end segment of y. Introducing the summing operator $\mathbf{s}$, a column vector with all entries equal to 1, eq 3.5 can be rewritten as

$$\frac{C_y}{n_y} = [\mathbf{s}^{T}\cdot\mathbf{g}(y,r_y)]^{-1} = [F_y]^{-1} \tag{B.7}$$

assuming that the end segment is free, and where F_y is introduced as a short-hand notation for the inverse of C_y/n_y which normalizes the end segment distribution of y. (If the end segment was confined to some layer i, $\mathbf{s}$ would be substituted for by the selection operator Δ_i which is a column vector with entries δ_{ij} ($j = 1, ..., M$).) If n_y is fixed, C_y is adjusted to satisfy eq B.7 and vice versa.

To obtain the distribution of the rest of the segment ranks, the $\mathbf{g}(y,s)$ resulting from a forward walk (eq B.6) needs to be renormalized, each with different correction factor. Using a method related to the procedure of Rubin and Di Marzio,[105] it has been shown[48] that these correction factors can be evaluated by a backward walk from the end segment to segment s. For component y, the total number of segments of rank s in layer i then becomes

$$n_{ysi} = C_y F_{ysi} B_{y,r-s+1,i} \tag{B.8}$$

where the forward walk F and the backward walk B are defined by

$$F_{ysi} \equiv \Delta_i^{T}\cdot[\prod_{s'=2}^{s}\mathbf{W}^{t(y,s')}]\cdot\mathbf{g}(y,1)$$

$$B_{y,r-s+1,i} \equiv \Delta_i^{T}\cdot[\prod_{s'=r_y}^{s}(\mathbf{W}^{t(y,s')})^{T}]\cdot\mathbf{s} \tag{B.9}$$

again assuming that the end segments are free. (Note the reverse order of the matrix multiplication for the backward walk.)

Equation B.8 is the central result, and all distributions are obtained by summing it in different ways. In particular, the number of species A in layer i is given by

$$n_{Ai} = \sum_y n_{yAi} = \sum_y C_y \sum_{s=1}^{r_y}\delta_{A,t(y,s)}F_{ysi}B_{y,r-s+1,i} \tag{B.10}$$

The corresponding volume fractions are given by $\Phi_{yAi} = n_{yAi}/L_i$, etc.

B.2. Equilibrium Internal State Distribution. The internal states are chosen so that the free energy is minimized for the specified "equilibrium" set of conformations. Consequently, the internal state distribution minimizes only A_{int} and U and is thus uniquely determined by the distribution of species. Since the probabilities should sum to 1

$$\sum_B P_{ABi} = 1 \tag{B.11}$$

a new unrestricted function g is formed using the Lagrange multipliers γ_{Ai}

$$g = U + A_{int} + \sum_A\sum_i \gamma_{Ai}[1 - \sum_B P_{ABi}] \tag{B.12}$$

Minimizing g with respect to P_{ABi} (using eqs 4.3 and 4.4) and eliminating a constant involving the Lagrange multipliers using the constraint in eq B.11, P_{ABi} is given by

$$P_{ABi} = \frac{g_{AB}\exp[-\beta U_{AB} + \sum_{A'}\sum_{B'}\chi_{BB'}\langle P_{A'B'i}\Phi_{A'i}\rangle]}{\sum_B g_{AB}\exp[-\beta U_{AB} + \sum_{A'}\sum_{B'}\chi_{BB'}\langle P_{A'B'i}\Phi_{A'i}\rangle]} \tag{B.13}$$

For most parameter choices with low coupling between states, P_{ABi} can be evaluated directly by insertion in a few iterations. The second derivative of g is clearly positive, ensuring a minimum in the free energy. It is not surprising to find that the normalizing factor turns out to be closely related to the weight factor G_{Ai}. Insertion of eq B.13 in the logarithmic term of eq 4.7 obtains

$$P_{ABi} = \frac{g_{AB}\exp[-\beta U_{AB} + \sum_{A'}\sum_{B'}\chi_{BB'}\langle P_{A'B'i}\Phi_{A'i}\rangle]}{\exp[-(\beta u_{Ai} + \alpha_i)]} \tag{B.14}$$

Appendix C. Numerical Tricks

In section 5, a self-consistent solution is reached when the chosen set of species potentials $\{\eta_{Ai}\}$ results in $\{n_{Ai}\}$ and $\{\alpha_{Ai}\}$ which satisfy eqs 5.1 and 5.2. Unfortunately the evaluation of $\{n_{Ai}\}$, as described in Appendix B, will encounter numerical problems unless the levels in the set $\{\eta_{Ai}\}$ are chosen wisely. The main problem is that the chemical potential of the polymers tends to be large (especially in confined systems). As a consequence, C_y ($\exp(\beta\eta_y)$) may cause numerical overflow, with a corresponding underflow in F_y (eq B.7). A natural solution is to transfer some of the excess from C_y to F_y. We have essentially adopted a method proposed by Evers et al.[49] Since this paper is somewhat different, it is presented in extenso. The object is to alleviate the numerical trouble by adjusting the weight factors so that all G_{Ai}' are on the order of 1 (shifted quantities are denoted by primes) while keeping track of the shifts to enable determination of $\{\alpha_{Ai}\}$.

A new set of iteration variables are defined by

$$x_{Ai} = -\beta[u_{Ai} - u_A^{ref} - \bar{u}] + \frac{\sum_y \ln F_y}{\sum_A\sum_i 1} \tag{C.1}$$

where u_{Ai} and F_y are given by eqs 4.7 and B.7, respectively. The species reference potential u_A^{ref} is zero except for species in components z which are in equilibrium with

another system (cf. section 6.2). It only depends on system two and is given by the average

$$u_A^{ref} = \frac{\sum_i u_{Ai}(\text{system two})}{\sum_i 1} \quad (C.2)$$

It is specifically introduced to prevent overflow in the fixed C_z. The fixed chemical potentials μ_z are reduced by the corresponding u_A^{ref} for each segment. The average species potential in the system of interest

$$\bar{u} = \frac{\sum_A \sum_i u_{Ai} - u_A^{ref}}{\sum_A \sum_i 1} \quad (C.3)$$

is subtracted to shift the first square bracket in eq C.1 into the neighborhood of zero. The last term in eq C.1 is introduced to enable extraction of the average species potential from the iteration variables (see below).

Since the average iteration variable is

$$\bar{x} = \frac{\sum_A \sum_i x_{Ai}}{\sum_A \sum_i} = \frac{\sum_y \ln F_y}{\sum_A \sum_i} \quad (C.4)$$

we can write the equality

$$x_{Ai} - \bar{x} = -\beta[u_{Ai} - u_A^{ref} - \bar{u}] \quad (C.5)$$

The shifted weight factors are then taken to be

$$G_{Ai}' = \exp(-\beta[u_{Ai} - u_A^{ref} - \bar{u}]) = \exp(x_{Ai} - \bar{x}) \quad (C.6)$$

where all G_{Ai}' are on the order of 1. These can now safely be used to evaluate the resulting $\{n_{Ai}\}$ by the procedure outlined in Appendix B.

Introducing the short-hand notation $\psi_{Ai} = \beta u_{Ai} + \alpha_i$ in eq 4.7 and noting that the average species potential is extracted from the iteration variables by

$$\beta\bar{u} = \frac{[\sum_y \ln F_y'] - [\sum_A \sum_i x_{Ai}] - [\sum_y \sum_{s=1}^{r_y} \beta u_{t(y,s)}^{ref}]}{\sum_y r_y} \quad (C.7)$$

each α_{Ai} can be written as

$$\alpha_{Ai} = [x_{Ai} - \bar{x}] - \beta u_A^{ref} - \beta\bar{u} + \psi_{Ai}[\sum_A \Phi_{Ai}]^{-1} \quad (C.8)$$

where the damping factor for ψ_{Ai} is a trick to reduce large oscillations when the weight factors are far from the solution.

Appendix D. Conformational Analysis

Once a self-consistent set of weight factors $\{G_{Ai}\}$ is found, probabilities of chain conformations can be analyzed through eq B.2. The information can be reduced by dividing the chains into four classes: free chains (f), chains absorbed only on surface s (a) *or* s′ (a′), and chains bridging s and s′ (b). Now, the external potential in section 4 (i.e., setting all weight factors outside the system to zero) was introduced to select all possible conformations of chains inside the confined system. Following Scheutjens and coworkers, the external potential may similarly be chosen to select another subset of chains. (A more detailed treatment is given in ref 49.) Thus, by setting all weight factors in layer 1 and M to zero, only free chains remain. Zeroing only those in layer M selects chains that are free or absorbed to surface s only, etc. By zeroing weight factors in either layer 1 or M, or both, or none, the proportions of the above classes may be evaluated by linear combination. The normalizing factors in eq B.7, abbreviated F_y, satisfy

$$F_y^t = F_y^f + F_y^a + F_y^{a'} + F_y^b \quad (D.1)$$

where t denotes the set of all chains. The probability that a chain of component y belongs to class c is then

$$P_y^c = \frac{F_y^c}{F_y^t} \quad (D.2)$$

and since eq B.8 using the above notation may be written as

$$n_{ysi}^t = C_y[F_{ysi}^f + F_{ysi}^a + F_{ysi}^{a'} + F_{ysi}^b][B_{y,r-s+1,i}^f + B_{y,r-s+1,i}^a + B_{y,r-s+1,i}^{a'} + B_{y,r-s+1,i}^b] \quad (D.3)$$

the segments of rank s in layer i may similarly be divided into classes. We group the 16 possibilities (in abbreviated form) into

ff	free
fa, af	tail from s
fa′, a′f	tail from s′
fb, bf	tail from s or s′
aa	loop or train on s
a′a′	loop or train on s′
aa′, a′a	single bridge
ab, a′b, bb, ba, ba′	loop and bridge or double bridge, i.e., the rest

For each class eq D.3 may be summed as in eq B.10 for the respective species distributions.

The hydrodynamic thickness (see ref 99 for details) is given by

$$\delta_h = M - \alpha(M) \quad (D.4)$$

where $\alpha(i)$ is recursively obtained through

$$\alpha(i) = \frac{q_i \tanh q_i^{-1} + \alpha(i-1)}{1 + \alpha(i-1)\, q_i^{-1} \tanh q_i^{-1}} \quad (D.5)$$

Since $\alpha(0) = 0$ and q_i is taken to be

$$q_i = \left(\frac{1 - \Phi_i^a}{\Phi_i^a}\right)^{1/2} \quad (D.6)$$

eq D.4 is readily evaluated. The volume fraction distribution Φ_i^a is in general the total contribution from all segments of absorbed components but can be restricted to the contributions from chains on *one* surface. In this paper the latter is used to probe the state of grafted chains.

Appendix E. Bulk System

Consider a bulk solution, where the Bragg–Williams approximation is applied over the whole system. In a treatment similar to that in sections 3–6, the canonical

chemical potential of a component y is

$$\beta\eta_y^{\,b} = \ln\frac{n_y}{V} - r_y\alpha + \sum_A\sum_B r_{yA}P_{AB}\left\{\beta U_{AB} + \ln\frac{P_{AB}}{g_{AB}} + \sum_{A'}\sum_{B'}\chi_{BB'}P_{A'B'}\Phi_{A'}\right\} \quad \text{(E.1)}$$

where r_{yA} is the number of segments of species type A in component y, V is the volume, and Φ_A is the volume fraction of species A. α is given by

$$\alpha = \left[\sum_x \frac{n_x}{V}\right] + \frac{1}{2}\sum_A\sum_B\sum_{A'}\sum_{B'}\Phi_A P_{AB}\chi_{BB'}P_{A'B'}\Phi_{A'} \quad \text{(E.2)}$$

in order to satisfy the Gibbs–Duhem relation. The derived chemical potential in eq E.1 can be shown to be equivalent to the one derived by Evers et al.[49] after a change is made to their reference state. For the special case of a bulk system of one pure component without internal degrees of freedom, the chemical potential becomes

$$\beta\eta_y^{\,b} = -\ln(r_y) - 1 \quad \text{(E.3)}$$

References and Notes

(1) Napper, D. H. *J. Colloid Interface Sci.* **1977**, *58*, 391.
(2) Napper, D. H. *Polymeric Stabilization of Colloidal Dispersions*; Academic Press: London, 1983.
(3) Alexander, S. *J. Phys. (Paris)* **1977**, *38*, 977.
(4) Alexander, S. *J. Phys. (Paris)* **1977**, *38*, 983.
(5) de Gennes, P.-G. *Scaling Concepts in Polymer Physics*; Cornell University Press: Ithaca, NY, 1979.
(6) de Gennes, P.-G. *Macromolecules* **1980**, *13*, 1069.
(7) de Gennes, P.-G. *Macromolecules* **1981**, *14*, 1637.
(8) de Gennes, P.-G. *Macromolecules* **1982**, *15*, 492.
(9) de Gennes, P.-G. *Adv. Colloid Interface Sci.* **1987**, *27*, 189.
(10) Leibler, L. *Macromolecules* **1980**, *13*, 1602.
(11) Klein, J.; Pincus, P. *Macromolecules* **1982**, *15*, 1129.
(12) Gast, A. P.; Leibler, L. *Macromolecules* **1986**, *19*, 686.
(13) Witten, T. A.; Pincus, P. A. *Macromolecules* **1986**, *19*, 2509.
(14) Leibler, L.; Pincus, P. A. *Macromolecules* **1986**, *19*, 2922.
(15) Ingersent, K.; Klein, J.; Pincus, P. *Macromolecules* **1986**, *19*, 1374.
(16) Bug, A. L. R.; Cates, M. E.; Safran, S. A.; Witten, T. A. *J. Chem. Phys.* **1988**, *88*, 1290.
(17) Patel, S.; Tirell, M.; Hadziioannou, G. *Colloids Surf.* **1988**, *31*, 157.
(18) Rossi, G.; Cates, M. E. *Macromolecules* **1988**, *21*, 1372.
(19) Helfand, E.; Tagami, Y. *J. Chem. Phys.* **1972**, *56*, 3592.
(20) Helfand, E. *J. Chem. Phys.* **1975**, *62*, 999.
(21) Dolan, A. K.; Edwards, S. F. *Proc. R. Soc. London A* **1974**, *337*, 509.
(22) Dolan, A. K.; Edwards, S. F. *Proc. R. Soc. London A* **1975**, *343*, 427.
(23) Muthukumar, M.; Ho, J.-S. *Macromolecules* **1989**, *22*, 965.
(24) Hong, K. M.; Noolandi, J. *Macromolecules* **1980**, *13*, 964.
(25) Evans, E. A. *Macromolecules* **1989**, *22*, 2277.
(26) Ploehn, H. J.; Russel, W. B.; Hall, C. K. *Macromolecules* **1988**, *21*, 1075.
(27) Ploehn, H. J.; Russel, W. B. *Macromolecules* **1989**, *22*, 266.
(28) Semenov, A. N. *Sov. Phys. JETP* **1985**, *61*, 733 (*Zh. Eksp. Theor. Fiz.* **1985**, *88*, 1242).
(29) Ohta, T.; Kawasaki, K. *Macromolecules* **1986**, *19*, 2621.
(30) Zhulina, E. B.; Birshtein, T. M. *Vysokomol. Soedin., Ser. A* **1986**, *28*, 2589.
(31) Zhulina, E. B.; Borisov, O. V.; Priamitsyn, V. A. *J. Colloid Interface Sci.* **1990**, *137*, 495.
(32) Zhulina, E. B.; Borisov, O. V.; Priamitsyn, V. A.; Birshtein, T. M. *Macromolecules* **1991**, *24*, 140.
(33) Milner, S. T.; Witten, T. A.; Cates, M. E. *Macromolecules* **1988**, *21*, 2610.
(34) Milner, S. T.; Witten, T. A.; Cates, M. E. *Macromolecules* **1989**, *22*, 489.
(35) Milner, S. T.; Witten, T. A.; Cates, M. E. *Macromolecules* **1989**, *22*, 853.
(36) Milner, S. T. *J. Chem. Soc., Faraday Trans.* **1990**, *86*, 1349.
(37) Ball, R. C.; Marko, J. F.; Milner, S. T.; Witten, T. A. *Macromolecules* **1991**, *24*, 693.
(38) Roe, R. J. *J. Chem. Phys.* **1974**, *60*, 4192.
(39) Helfand, E. *J. Chem. Phys.* **1975**, *63*, 2192.
(40) Scheutjens, J. M. H. M.; Fleer, G. J. *J. Phys. Chem.* **1979**, *83*, 1619.
(41) Scheutjens, J. M. H. M.; Fleer, G. J. *J. Phys. Chem.* **1980**, *84*, 1882.
(42) Scheutjens, J. M. H. M.; Fleer, G. J. *Macromolecules* **1985**, *18*, 1882.
(43) Cosgrove, T.; Heath, T.; Van Lent, B.; Leermakers, F.; Scheutjens, J. *Macromolecules* **1987**, *20*, 1692.
(44) Wang, Z.-G.; Rice, S. A. *J. Chem. Phys.* **1988**, *88*, 1290.
(45) Van Lent, B.; Scheutjens, J. M. H. M. *Macromolecules* **1989**, *22*, 1931.
(46) Leermakers, F. A. M.; Scheutjens, J. M. H. M. *J. Phys. Chem.* **1989**, *93*, 7417.
(47) Van Lent, B.; Israels, R.; Scheutjens, J. M. H. M.; Fleer, G. J. *J. Colloid Interface Sci.* **1990**, *137*, 380.
(48) Björling, M.; Linse, P.; Karlström, G. *J. Phys. Chem.* **1990**, *94*, 471.
(49) Evers, O. A.; Scheutjens, J. M. H. M.; Fleer, G. J. *Macromolecules* **1990**, *23*, 5221.
(50) Evers, O. A.; Scheutjens, J. M. H. M.; Fleer, G. J. *J. Chem. Soc., Faraday Trans.* **1990**, *86*, 1333.
(51) Evers, O. A.; Scheutjens, J. M. H. M.; Fleer, G. J. *Macromolecules* **1991**, *24*, 5558.
(52) Linse, P.; Björling, M. *Macromolecules* **1991**, *24*, 6700.
(53) Marčelja, S. *Biochim. Biophys. Acta* **1974**, *367*, 165.
(54) Gruen, D. W. R. *Biochim. Biophys. Acta* **1980**, *595*, 161.
(55) Gruen, D. W. R. *J. Colloid Interface Sci.* **1981**, *84*, 281.
(56) Gruen, D. W. R. *J. Phys. Chem.* **1985**, *89*, 146.
(57) Gruen, D. W. R. *J. Phys. Chem.* **1985**, *89*, 153.
(58) Ben-Shaul, A.; Szleifer, I.; Gelbart, W. M. *J. Chem. Phys.* **1985**, *83*, 3597.
(59) Szleifer, I.; Ben-Shaul, A.; Gelbart, W. M. *J. Chem. Phys.* **1985**, *83*, 3612.
(60) Szleifer, I.; Ben-Shaul, A.; Gelbart, W. M. *J. Chem. Phys.* **1986**, *85*, 5345.
(61) Szleifer, I.; Ben-Shaul, A.; Gelbart, W. M. *J. Chem. Phys.* **1987**, *86*, 7094.
(62) Theodorou, D. N. *Macromolecules* **1988**, *21*, 1391.
(63) Theodorou, D. N. *Macromolecules* **1988**, *21*, 1400.
(64) Marquese, J.; Dill, K. A. *J. Chem. Phys.* **1986**, *85*, 434.
(65) Naghizadeh, J.; Dill, K. A. *Macromolecules* **1991**, *24*, 1768.
(66) Israelachvili, J. N.; Adams, G. E. *J. Chem. Soc., Faraday Trans. 1* **1978**, *74*, 975.
(67) Klein, J.; Luckham, P. *Nature* **1982**, *300*, 429.
(68) Klein, J. *J. Chem. Soc., Faraday Trans. 1* **1983**, *79*, 99.
(69) Klein, J.; Luckham, P. F. *Macromolecules* **1984**, *17*, 1041.
(70) Israelachvili, J. N.; Tirell, M.; Klein, J.; Almog, Y. *Macromolecules* **1984**, *17*, 204.
(71) Luckham, P. F.; Klein, J. *Macromolecules* **1985**, *18*, 721.
(72) Luckham, P. F.; Klein, J. *J. Chem. Soc., Faraday Trans.* **1990**, *86*, 1363.
(73) Claesson, P. M.; Kjellander, R.; Stenius, P.; Christenson, H. K. *J. Chem. Soc., Faraday Trans. 1* **1986**, *82*, 2735.
(74) Claesson, P. M.; Gölander, C.-G. *J. Colloid Interface Sci.* **1986**, *117*, 366.
(75) Hadziioannou, G.; Patel, S.; Granick, S.; Tirell, M. *J. Am. Chem. Soc.* **1986**, *108*, 2869.
(76) Ansarifar, M. A.; Luckham, P. F. *Polymer* **1988**, *29*, 329.
(77) Marra, J.; Hair, M. L. *Colloids Surf.* **1988/89**, *34*, 215.
(78) Taunton, H. J.; Toprakcioglu, C.; Fetters, L. J.; Klein, J. *Macromolecules* **1990**, *23*, 571.
(79) Guzonas, D.; Boils, D.; Hair, M. L. *Macromolecules* **1991**, *24*, 3383.
(80) Dai, L.; Toprakcioglu, C. Preprint.
(81) Malmsten, M.; Claesson, P. M.; Pezron, E.; Pezron, I. *Langmuir* **1990**, *6*, 1572.
(82) Malmsten, M.; Claesson, P. M. *Langmuir* **1991**, *7*, 988.
(83) Flory, J. P. *Principles of Polymer Chemistry*; Cornell University Press: Ithaca NY, 1953.
(84) Freed, K. F. *Renormalization Group Theory of Macromolecules*; Wiley: New York, 1987; Chapter 4.
(85) Andersson, M.; Karlström, G. *J. Phys. Chem.* **1985**, *89*, 4957. Karlström, G. *J. Phys. Chem.* **1985**, *89*, 4962.
(86) Björling, M.; Karlström, G.; Linse, P. *J. Phys. Chem.* **1991**, *95*, 6706.
(87) Tiberg, F.; Malmsten, M.; Linse, P.; Lindman, B. Submitted to *Langmuir*.
(88) Björling, M.; Linse, P. Submitted to *J. Chem. Phys.*
(89) Silberberg, A. J. *J. Chem. Phys.* **1962**, *66*, 1872.
(90) Friedman, H. L. *A Course in Statistical Mechanics*; Prentice-Hall: Englewood Cliffs, NJ, 1985.
(91) Plischke, M.; Bergersen, B. *Equilibrium Statistical Physics*; Prentice-Hall: Englewood Cliffs, NJ, 1989.

(92) Press, W. H.; Flannery, B. P.; Teukolsky, S. A.; Vetterling, W. T. *Numerical Recipes*; Cambridge University Press: New York, 1986.
(93) Israelachvili, J. N. *Intermolecular and Surface Forces*; Academic Press: London, 1985.
(94) Hill, T. L. *An Introduction to Statistical Thermodynamics*; Dover: New York, 1986; Chapter 16.
(95) Fouss, R. M.; Katchalsky, A.; Lifson, S. *Proc. Natl. Acad. Sci. U.S.A.* **1951**, *37*, 579.
(96) Marcus, R. A. *J. Chem. Phys.* **1955**, *23*, 1057.
(97) Gunnarsson, G.; Jönsson, Be.; Wennerström, H. *J. Phys. Chem.* **1980**, *84*, 3114.
(98) Israelachvili, J. N.; Wennerström, H. *Langmuir* **1990**, *6*, 873.
(99) Scheutjens, J. M. H. M.; Fleer, G. J.; Cohen Stuart, M. A. *Colloids Surf.* **1986**, *21*, 285.
(100) Miklavic, S. J.; Woodward, C. E.; Jönsson, Be.; Akesson, T. *Macromolecules* **1990**, *23*, 4149.
(101) Shinoda, K. *J. Phys. Chem.* **1977**, *81*, 1300.
(102) Clunie, J. S.; Goodman, J. F.; Symons, P. C. *Trans. Faraday Soc.* **1969**, *65*, 287.
(103) Mitchell, D. J.; Tiddy, G. J. T.; Waring, L.; Bostock, T.; McDonald, M. P. *J. Chem. Soc., Faraday Trans. 1* **1983**, *79*, 975.
(104) Lindman, B.; Wennerström, H. *J. Phys. Chem.* **1991**, *95*, 6053.
(105) Rubin, R. J.; Di Marzio, E. A. *J. Chem. Phys.* **1971**, *55*, 4318.

Registry No. PEO, 25322-68-3.